

Orthogonal Alignment of Galaxy Group Angular Momentum with Cosmic Filament Spines: An Observational Study

YU RONG,^{1,2} PENG WANG,³ AND XIAO-XIAO TANG^{3,4}

¹*Department of Astronomy, University of Science and Technology of China, Hefei, Anhui 230026, People's Republic of China*

²*School of Astronomy and Space Sciences, University of Science and Technology of China, Hefei 230026, Anhui, People's Republic of China*

³*Shanghai Astronomical Observatory, Chinese Academy of Sciences, Nandan Road 80, Shanghai 200030, People's Republic of China*

⁴*University of Chinese Academy of Sciences, Beijing 100049, China*

(Received March 10, 2025; Revised tomorrow; Accepted the day after tomorrow)

Submitted to ApJ Letters

ABSTRACT

We investigate the alignment between the angular momenta of galaxy groups and the spines of their associated cosmic filaments. Our results demonstrate a significant tendency for these two orientations to be perpendicular, indicating that the rotation of a galaxy group does not originate from the spin of cosmic filaments. Instead, it is driven by the orbital angular momentum contributed by member galaxies as they accrete along the direction of the filament spines. Moreover, the strength of this perpendicular alignment signal varies with the richness of the galaxy groups, with the most pronounced alignment observed among the wealthiest groups. This pronounced alignment is largely due to the more coherent spatial distribution of member galaxies in richer groups relative to the filament spines. Our study provides valuable insights into the mechanisms of angular momentum acquisition in galaxy groups from an observational standpoint.

Keywords: galaxies: formation — galaxies: evolution — methods: statistical — galaxies: photometry

1. INTRODUCTION

The hierarchical genesis of cosmic structures, ranging from small-scale galaxy pairs to large-scale galaxy clusters and groups, constitutes a fundamental aspect of our understanding of cosmic evolution. According to the hierarchical evolution theory of cosmic structures, galaxy clusters and groups gradually form through the amalgamation of individual galaxies originating from large-scale filaments. Investigating these cosmic entities yields invaluable insights into both the formation and evolution of the galaxies they encompass and the large-scale structures themselves.

Galaxy clusters and groups represent the largest virialized structures in the universe, containing hundreds to thousands of galaxies. A pivotal aspect of these structures is their angular momentum properties. The angular momentum of a galaxy cluster or group, which encapsulates the collective rotational motion of its constituent galaxies, serves as a crucial parameter for elucidating the complex dynamics and evolutionary trajectories of these cosmic structures. A pertinent question arises regarding the origins of the angular momentum in galaxy groups and clusters. Recent observational studies (Wang et al. 2021; Tang et al. 2025) indicate that large-

scale filaments exhibit self-rotation, with their rotation axes aligned with their spines (see Fig. 1). As nodes at which filaments converge, galaxy clusters and groups may inherit the rotational angular momentum direction from these filaments, suggesting that the angular momentum direction of galaxy clusters and groups could be in principle aligned parallel to the direction of the filament spines.

Conversely, investigations into galaxy pairs and triplets reveal that their systemic angular momentum tends to be perpendicular to the direction of the filament spines, attributed to the distribution of member galaxies along these structures (Tempel & Tamm 2015; Rong et al. 2024). For massive galaxy clusters and groups, given that their member galaxies predominantly accrete along the filaments, one might expect a similar distribution along the direction of the filament spines (e.g., Knebe et al. 2004). However, due to the large number of member galaxies, the overall angular momentum direction of the system may exhibit greater complexity, and could potentially lack a clear correlation with the filament direction.

A systematic investigation into the angular momentum alignment within virialized systems of varying scales, in relation to their associated filaments, yields essential insights into the fundamental mechanisms that govern their formation and evolution. Over the past decade, the relationship between the angular momentum orientations of galaxies, which represent small virialized units, and cosmic filaments has been

extensively studied. Cosmological simulations have demonstrated that the angular momentum of low-mass galaxy halos tends to align their spin directions parallel to the filament spines, likely due to anisotropic collapse and tidal torques (Codis et al. 2012; Laigle et al. 2015; Libeskind et al. 2013; Ganeshiaiah Veena et al. 2019; Barsanti et al. 2022; Kraljic et al. 2021; Tempel et al. 2013; Tempel & Libeskind 2013; Zhang et al. 2015; Dubois et al. 2014; Wang & Kang 2017, 2018). In contrast, the angular momentum of high-mass halos is more frequently oriented perpendicular to the filament spines. This phenomenon arises because these systems form primarily through galaxy mergers, which predominantly occur along the direction of the filament spines due to the spatial distribution of galaxies along these structures (Lee & Choi 2015; Tempel et al. 2015; Wang & Kang 2018). As a result, the orbital angular momentum associated with these mergers tends to be perpendicular to the filament spines; following the merger, this orbital angular momentum is transformed into the rotational angular momentum of the resultant halo, thereby aligning it perpendicular to the filament spine (Tempel et al. 2013; Tempel & Libeskind 2013; Tempel et al. 2015; Barsanti et al. 2022; Kraljic et al. 2021; Kitzbichler & Saurer 2003; Rong et al. 2015b, 2016; Rong & Wang 2024).

This study aims to investigate the alignment of angular momentum in galaxy groups within cosmic filaments in observations. Section 2 outlines the sample utilized in this investigation. Section 3 presents the methodology for estimating the rotation axes of galaxy groups as viewed on the celestial plane. Section 4 analyzes the alignment between the angular momentum vectors and filament spines on the celestial plane. Finally, Sections 5 and 6 provide a discussion and summary of the findings, respectively.

2. SAMPLE

We employ the spectroscopic galaxy sample curated by Tempel et al. (2012), which is based on data from the Sloan Digital Sky Survey (SDSS; Aihara et al. 2011). This sample is confined to an r -band Petrosian magnitude threshold of $m_r = 17.77$ mag and encompasses a variety of properties for each galaxy, including its spatial coordinates, $ugriz$ -band absolute magnitudes, group ranking (‘rank’), and other pertinent characteristics. The identification of galaxy groups and clusters was accomplished in the work of Tempel et al. (2012) using the friends-of-friends (FOF) algorithm, which yielded estimates of the richness and virial radius for each galaxy group or cluster.

For every galaxy member within a group, the stellar mass, M_* , is estimated from the r -band absolute magnitude and $g - r$ color, utilizing the mass-to-light ratio described by $\log(M_*/L_r) = 1.097(g - r) - 0.306$ (Bell et al. 2003). This method for estimating stellar mass based on color carries a typical uncertainty of approximately 0.10-0.15 dex. In this study, we designate the galaxies with ‘rank=1’, i.e. the brightest members, as the centers of their respective groups. We have verified that using the most massive members as group centers would not alter any of our conclusions.

In a Cartesian coordinate system, the position of the i -th member galaxy in a group within a group on the celestial plane is determined using the methodology delineated by Tempel et al. (2014), expressed as,

$$\begin{aligned} x_i &= -\sin \lambda_i, \\ y_i &= \cos \lambda_i \cos \eta_i, \\ z_i &= \cos \lambda_i \sin \eta_i, \\ \mathbf{r}_i &= [x_i, y_i, z_i] - [x_c, y_c, z_c], \end{aligned} \quad (1)$$

where λ_i and η_i denote the SDSS survey coordinates of the i -th member galaxy. The vector $\mathbf{e}_c = [x_c, y_c, z_c]$ represents the position vector of the group center, while \mathbf{r}_i describes the position vector of the i -th member relative to the group center on the celestial plane.

The filament associated with each galaxy group is identified using the filament catalog compiled by Tempel et al. (2014), based on the three-dimensional distance d_{gf} from the center of the group to the spine of the filament. The alignment analysis is confined to groups for which $d_{\text{gf}} \leq 1.0$ Mpc/ h , which approximately delineates a filament boundary (Wang et al. 2024). This final sample comprises 30,880 galaxy groups situated within their corresponding host filaments.

The three-dimensional (3D) orientation of the spine of the filament, associated with each galaxy group, is provided by Tempel et al. (2014). The orientation of the nearest filament point is adopted as the orientation of the filament spine, denoted as $\mathbf{e}_f = [dx, dy, dz]$. For further details on the methodology for estimating the 3D orientations of cosmic filaments, we direct readers to Tempel et al. (2014).

3. GROUP ANGULAR MOMENTUM

In this study, we investigate the potential alignment between the angular momenta of galaxy groups, denoted as \mathbf{L} , and the spine orientations of their parent cosmic filaments, represented as \mathbf{e}_f . We note that, if the two vectors exhibit parallelism or orthogonality in 3D space, we expect to observe corresponding signals of parallelism or orthogonality on the two-dimensional (2D) celestial plane. To mitigate potential systematic biases arising from distances derived from redshift measurements, we focus our investigation on alignment signals within the celestial plane.

The filament orientation vector \mathbf{e}_f is projected onto the celestial plane as,

$$\begin{aligned} \mathbf{e}'_f &= \mathbf{e}_f - (\mathbf{e}_f \cdot \mathbf{e}_c) \mathbf{e}_c, \\ \mathbf{e}'_f &= \mathbf{e}'_f / |\mathbf{e}'_f|. \end{aligned} \quad (2)$$

We then define the component of \mathbf{L} in the celestial plane, \mathbf{L}_p , as

$$\begin{aligned} \mathbf{L}_p &\equiv \sum_{i=1}^N M_i \mathbf{r}_i \times \mathbf{v}_i, \\ \mathbf{e}_{L_p} &= \mathbf{L}_p / |\mathbf{L}_p|, \end{aligned} \quad (3)$$

where N denotes the richness of a group, M_i represents the mass weight of the i -th member galaxy, \mathbf{v}_i indicates the relative radial velocity vector of the i -th member galaxy along

the line of sight, defined as

$$\mathbf{v}_i = (v_i - v_c)[x_i, y_i, z_i], \quad (4)$$

with v_i and v_c denoting the radial velocities of the i -th member galaxy and the brightest galaxy in the group, respectively. These velocities are derived from the spectroscopically observed redshifts z_{obs} , according to the relation $v \simeq cz_{\text{obs}}$, where c is the speed of light.

The observational quantity L_p is perpendicular to the line-of-sight, thereby facilitating the characterization of the rotational motion of a galaxy group along this axis; it effectively represents the rotation axis of the group within the celestial plane. In section 5, we will elucidate that if \mathbf{L} and \mathbf{e}_f exhibit parallelism or orthogonality in 3D space, e_{Lp} and e'_f similarly exhibit parallelism or orthogonality in the 2D projection.

4. ALIGNMENT OF GROUP ANGULAR MOMENTUM WITH FILAMENT

Here, we assume the mass weight $M_i = M_*$. Subsequently, the intersection angle δ between e_{Lp} of each group and the projected filament vector e'_f is computed as

$$\delta = \arccos(e_{Lp} \cdot e'_f). \quad (5)$$

The angle δ is constrained within the interval $[0, 90^\circ]$.

In panel a of Fig. 2, we illustrate the distribution of δ for galaxy groups categorized by richness: groups with rich memberships (i.e., $N > 10$; 1,356 groups), those of intermediate richness (i.e., $3 < N \leq 10$; 8,557 groups), and groups with poor memberships (i.e., $2 \leq N \leq 3$; 20,967 groups). The distributions of δ for these three subsamples display a significant deviation from a uniform distribution, evidenced by Kolmogorov–Smirnov (K-S) test (compared to a uniform distribution) p -values of 10^{-18} , 10^{-54} , and 10^{-70} , respectively.

Following the methodology delineated in (Rong & Wang 2024, see also Rong et al. (2019, 2024)), we define the index $\mathcal{I}(\delta) = N_{0-45}/N_{45-90}$, where N_{0-45} and N_{45-90} signify the counts of galaxies with δ falling within the ranges $[0, 45^\circ]$ and $[45^\circ, 90^\circ]$, respectively. The uncertainty associated with $\mathcal{I}(\delta)$ is estimated via bootstrap resampling. From the original sample, consisting of k members, we randomly select k galaxies with replacement, iterating this procedure 1,000 times to derive 1,000 values for $\mathcal{I}(\delta)$. The standard deviation ($\sigma_{\mathcal{I}}$) of these values is subsequently used as a measure of uncertainty. A uniform distribution would yield $\mathcal{I}(\delta) \simeq 1$. Our findings reveal $\mathcal{I}(\delta) = 0.64 \pm 0.04$, 0.71 ± 0.02 , and 0.80 ± 0.01 for the subsamples of $N > 10$, $3 < N \leq 10$, and $2 \leq N \leq 3$, respectively. These results indicate a trend toward δ approaching 90° , suggesting a significant perpendicular alignment between the angular momenta of the groups and the cosmic filament spines, at a high level of confidence¹.

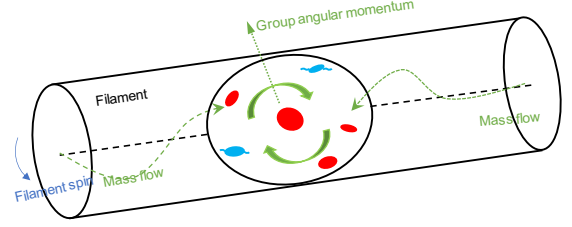


Figure 1. Schematic representation of a galaxy group and a segment of its associated large-scale filament. The galaxy group is depicted as a black ellipse, while a segment of the large-scale filament is illustrated as a black cylinder. Individual member galaxies within the group are represented by red and blue ellipses. The angular momentum of the group is indicated by dotted green arrows, and the mass flows relative to the galaxy group, signifying the infall of galaxies, are shown by dashed green arrows. The spin of the filament segment is denoted by a blue arrow.

Moreover, our analysis reveals the most pronounced alignment signal (i.e., the lowest $\mathcal{I}(\delta)$) within the subgroup characterized by rich memberships ($N > 10$) members, accompanied by a noticeable reduction in the strength of this signal as group richness decreases. Given that previous studies have indicated a strong dependence of group mass on richness (e.g., Plionis et al. 2006; Tovmassian & Plionis 2009), this trend also implies a diminishing alignment signal correlated with decreasing group mass.

Collectively, these observations support the hypothesis that a group’s angular momentum is predominantly influenced by the infall of its constituent galaxies, rather than inheriting rotation from the filament structures. Given that galaxies generally fall into groups in alignment with the filament direction (e.g., Tempel & Tamm 2015; Rong et al. 2024), it is expected that the direction of angular momentum would be perpendicular to the filament spine, as depicted in the accompanying diagram in Fig. 1.

5. DISCUSSION

5.1. Does result depend on weights?

In equation (3), we incorporate the mass and radius of each member galaxy as “weights” to determine the projected rotation axis of a galaxy group. It is important to acknowledge that galaxies situated at the periphery of a group are more likely to be misclassified as group members. In other words, galaxies with larger magnitudes of $|\mathbf{r}_i|$ are at an increased risk of erroneous classification (Serra & Diaferio 2013). This misidentification can lead to inaccuracies in the determination of the rotation axis in the celestial plane. Consequently, paralleling the methodology employed by Rong (2024), we also consider the application of mass weights exclusively, modifying equation (3) to

$$\begin{aligned} \mathbf{L}'_p &\equiv \sum_{i=1}^N \frac{M_i}{|\mathbf{r}_i|} \mathbf{r}_i \times \mathbf{v}_i, \\ e'_{Lp} &\equiv \mathbf{L}'_p / |\mathbf{L}'_p|. \end{aligned} \quad (6)$$

¹ The confidence level of an alignment signal is estimated as $|1 - \mathcal{I}(\delta)|/\sigma_{\mathcal{I}}$.

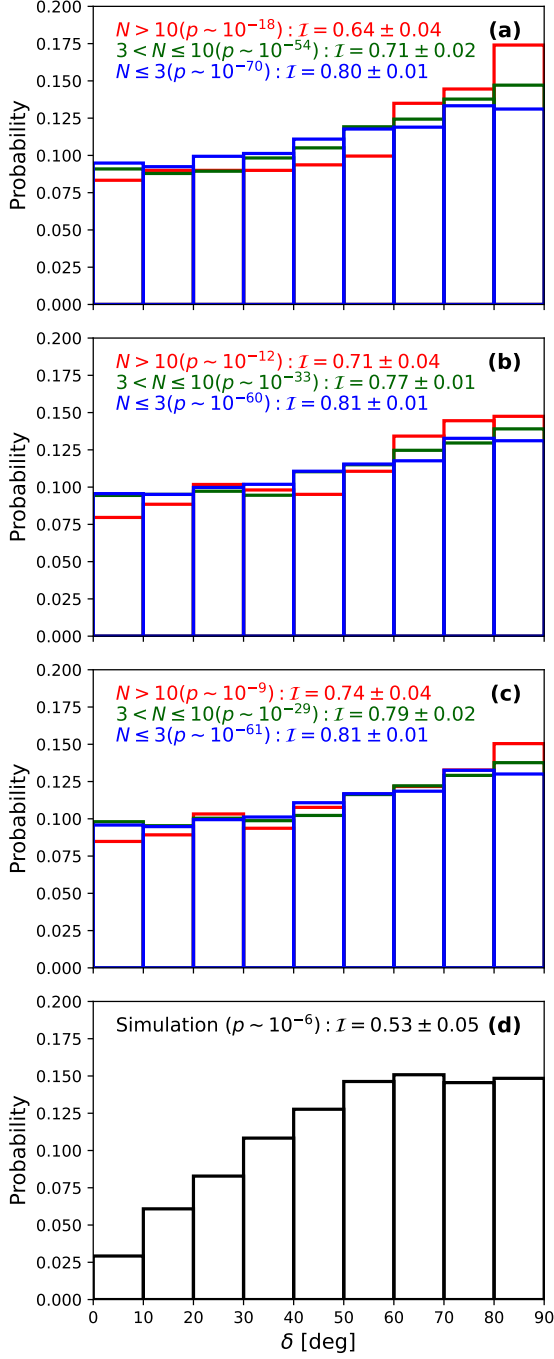


Figure 2. Panels a, b, and c illustrate the distributions of δ for galaxy groups categorized by member richness: groups with rich members ($N > 10$; red histogram), those of intermediate richness ($3 < N \leq 10$; green histogram), and groups with poor members ($2 \leq N \leq 3$; blue histogram). The analyses detailed in these panels employ various weighting schemes: panel a incorporates both mass and radius weights of member galaxies, panel b utilizes only the mass weights, and panel c assigns equal weights to all members. Panel d assesses the alignment in the 2D plane, evaluating whether the angular momenta of groups exhibit perpendicular alignment with the filament spines in 3D space, as derived from the Millennium-II simulation. The K-S test p -values of comparing the distributions and a uniform distribution are presented, alongside the values of $\mathcal{I}(\delta)$, highlighting the significance of the observed alignment.

The intersection angle between the projected rotation axis and the projected filament vector is then expressed as,

$$\delta' = \text{acos}(e'_{Lp} \cdot e'_f). \quad (7)$$

As depicted in panel b of Fig. 2, we observe a consistent pattern in the results, reinforcing the conclusion that the rotational direction of the galaxy group tends to be perpendicular to the orientation of the filament spine.

Additionally, we present the alignment results without applying any weighting to the member galaxies, effectively setting $M_i = 1$ for each member in equation (6). As illustrated in panel c of Fig. 2, the perpendicular alignment signal remains clearly evident.

Upon comparing the results in panels a, b, and c of Fig. 2, we find that, irrespective of the weighting scheme employed, the angular momentum alignment signal in more richly populated groups consistently exhibits greater strength. This observation suggests that the pronounced alignment in wealthier groups may primarily stem from the spatial distributions of member galaxies being more closely aligned with the filament spine, rather than arising from variations in the weighting scheme itself. In other words, richer groups may exhibit a more elliptical morphology, a conclusion supported by earlier studies (e.g., Wang et al. 2008).

5.2. Does the 2D result reveal the 3D case?

In section 2, we elucidate that if the rotation axis of a galaxy group in 3D space is perpendicular to the filament spine, then the rotation axis deduced from the 2D projection plane (celestial plane) using line-of-sight velocities will also align perpendicularly to the projected direction of the filament spine in the celestial plane. To substantiate this assertion, we quantitatively demonstrate the relationship using results from the Millennium-II N -body simulation (Boylan-Kolchin et al. 2009). In this simulation, halos and subhalos are identified using the FOF algorithm (Davis et al. 1985) and SUBFIND algorithm (Springel et al. 2001), respectively.

Initially, we compute the angular momentum \mathbf{L}_s of each halo (i.e., galaxy group) at redshift $z \sim 0$ in the 3D space, utilizing the 3D velocities of the member subhalos. We restrict our analysis to halos with masses exceeding $10^{13} M_\odot/h$ and subhalos with masses greater than $10^{10} M_\odot/h$ due to the limitations of simulation resolution. For the purpose of this investigation, we assume that the direction of the filament spine associated with each halo is strictly perpendicular to its angular momentum vector \mathbf{L}_s , with the spine oriented arbitrarily within the plane orthogonal to \mathbf{L}_s . We then project the spine onto the $y - z$ plane (with the x -axis representing the line-of-sight direction), designating it as e'_{sf} . Following the procedure outlined in equation (3), we compute the rotation axis of each halo in the $y - z$ plane, denoted as e_{Lsp} , by considering solely the velocity components of the member subhalos along the x -direction. Subsequently, we determine the angle δ_s between e'_{sf} and e_{Lsp} .

As illustrated in panel d of Fig. 2, δ_s approaches 90° , thereby indicating that if the angular momentum of the

galaxy group in 3D space is indeed perpendicular to the filament spine direction, the rotation axis of the galaxy group in 2D space is likewise oriented perpendicularly to the projected filament spine. Consequently, the results derived from the 2D analysis can accurately reflect the 3D case.

6. SUMMARY

Utilizing the galaxy group catalog and member galaxy data from SDSS, we investigate the alignment of the angular momenta of galaxy groups with the spines of their associated cosmic filaments as observed in the local universe. Our analysis concentrates on the alignment within the 2D celestial plane, and we examine various weighting methods to estimate the rotation axis of each group in this projection.

Our findings demonstrate that the rotation axes of galaxy groups consistently exhibit a tendency to be perpendicular to the projected filament spines, achieving a high level of statistical confidence regardless of the weighting methodologies employed. This observation suggests that, in 3D space, the angular momentum vectors of galaxy groups are likely aligned perpendicularly to their corresponding filament spines.

Moreover, the strength of the perpendicular alignment signal varies with the richness of the galaxy groups, with the most pronounced signals observed among the richest groups. For those groups containing more than 10 member galaxies, the alignment signal attains an approximate significance of 9σ . The enhanced signal in wealthier groups may be attributed to the fact that the distributions of member galaxies within these groups are more closely aligned with the fila-

ment spines. In our subsequent research, we will build upon the findings of this study by utilizing simulations to further investigate the perpendicular alignment between the angular momentum of galaxy groups and their associated filament spines (Tang et al., in preparation). Specifically, we aim to elucidate the mechanisms underlying the stronger alignment signal observed in galaxy groups of greater richness through simulation-based analyses.

This study offers valuable insights into the mechanisms by which angular momentum is acquired in galaxy groups from an observational perspective: the rotation is not inherited from cosmic filaments but instead arises from the orbital angular momentum imparted by member galaxies as they fall along the direction of the filament spines. Looking forward, we intend to compare these observational results with theoretical models, including frameworks that consider cold dark matter and warm dark matter, to enhance our understanding of the dynamics of dark matter.

Y.R. acknowledges supports from the CAS Pioneer Hundred Talents Program (Category B), the NSFC grant (No. 12273037), the USTC Research Funds of the Double First-Class Initiative, and the research grants from the China Manned Space Project (the second-stage CSST science projects: “Investigation of small-scale structures in galaxies and forecasting of observations” and “CSST study on specialized galaxies in ultraviolet and multi-band”). P.W. and XXT acknowledge financial support by the NSFC (No. 12473009), and also sponsored by Shanghai Rising-Star Program (No.24QA2711100).

REFERENCES

- Aihara, H., Allende Prieto, C., An, D., et al. 2011, *ApJS*, 193, 29
- Barsanti, S., et al. 2022, *MNRAS*, 516, 3569
- Bell, E. F., McIntosh, D. H., Katz, N., Weinberg, M. D. 2003, *ApJS*, 149, 289
- Boylan-Kolchin M., Springel V., White S. D. M., Jenkins A., Lemson G., 2009, *MNRAS*, 398, 1150
- Chen, Y.-C., Ho, S., Blazek, J., He, S., Mandelbaum, R., Melchior, P., Singh, S. 2019, *MNRAS*, 485, 2492
- Codis, S., Pichon, C., Devriendt, J., Slyz, A., Pogosyan, D., Dubois, Y., Sousbie, T., 2012, *MNRAS*, 427, 3320
- Coutts A., 1996, *MNRAS*, 278, 87
- Davis M., Efstathiou G., Frenk C. S., White S. D. M., 1985, *ApJ*, 292, 371
- de Vaucouleurs, G. 1948, *Ann. d’Ap.*, 11, 247
- Deng, X.-F., He, J.-Z., Wu, P., Ding, Y.-P. 2009, *ApJ*, 699, 948
- Dubois, Y., Pichon, C., Welker, C., et al. 2014, *MNRAS*, 444, 1453
- Ganeshiah Veena, P., Cautun, M., Tempel, E., van de Weygaert, R., Frenk, C. S. 2019, *MNRAS*, 487, 1607
- Hirata C. M., Seljak U., 2004, *Phys. Rev. D*, 70, 063526
- Hung L.-W., Bañados E., De Propris R., West M. J., 2010, *ApJ*, 720, 1483
- Kitzbichler, M. G., Saurer, W. 2003, *ApJ*, 590, L9
- Knebe, A., Gill, S. P. D., Gibson, B. K., Lewis, G. F., Ibata, R. A., Dopita, M. A. 2004, *ApJ*, 603, 7
- Kormendy, J. 2013, *Secular Evolution of Galaxies*, by Jesús Falcón-Barroso, and Johan H. Knapen, Cambridge, UK: Cambridge University Press, 2013, p.1
- Kraljic, K., et al. 2021, *MNRAS*, 504, 4626
- Laigle, C., et al. 2015, *MNRAS*, 446, 2744
- Lee, J., Choi, Y.-Y. 2015, *ApJ*, 799, 212
- Li, F., Wang, E., Zhu, M., et al. 2024, *ApJ*, 974, 238
- Libeskind, N. I., Hoffman, Y., Steinmetz, M., Gottlöber, S., Knebe, A., Hess, S., 2013, *ApJ*, 766, L15
- Maller, A. H., & Dekel, A. 2002, *MNRAS*, 335, 487
- Merluzzi, P. et al. 2015, *MNRAS*, 446, 803
- O’Kane, C. J., Kuchner, U., Gray, M. E., Aragón-Salamanca, A. 2024, *MNRAS*, 534, 1682
- Papastergis, E., Giovanelli, R., Haynes, M. P., Rodríguez-Puebla, A., Jones, M. G. 2013, *ApJ*, 776, 43

- Pereira, M. J., Kuhn, J. R. 2005, *ApJ*, 627L, 21
- Plionis M., Benoist C., Maurogordato S., Ferrari, C., Basilakos, S., 2003, *ApJ*, 594, 144
- Plionis M., Bryan, G. L., Ragone-Figueroa, C. 2006, *ApJ*, 650, 770
- Plionis M., Basilakos S., 2002, *MNRAS*, 329, L47
- Primack, J. R. 2024, *Annual Review of Nuclear and Particle Science*, 74, 173
- Rong, Y., Puzia, T. H., et al. 2019, *ApJ*, 883, 56
- Rong, Y. 2024, *Universe*, 10, 286
- Rong, Y., Shen, J., Hua, Z. 2024, *MNRAS*, 531L, 9
- Rong, Y., Liu, Y., Zhang, S.-N. 2016, *MNRAS*, 455, 2267
- Rong, Y., Wang, P. 2024, *arXiv*: 2411.14885
- Rong, Y., Yi, S.-X., Zhang, S.-N., Tu, H. 2015a, *MNRAS*, 451, 2536
- Rong, Y., Zhang, S.-N., Liao, J.-Y. 2015b, *MNRAS*, 453, 1577
- Schneider, M. D., et al. 2013, *MNRAS*, 433, 2727
- Serra, A. L., Diaferio, A. 2013, *ApJ*, 768, 116
- Springel V., White S. D. M., Tormen G., Kauffmann G., 2001, *MNRAS*, 328, 726
- Tang, X., Wang, P. et al. submitted
- Tempel, E., Guo, Q., Kipper, R., Libeskind, N. I. 2015, *MNRAS*, 450, 2727
- Tempel, E., Stoica, R. S., Saar, E. 2013, *MNRAS*, 428, 1827
- Tempel, E., Libeskind, N. I. 2013, *ApJ*, 775, L42
- Tempel, E., Stoica, R. S., Martínez, V. J., Liivamägi, L. J., Castellán, G., Saar, E., 2014, *MNRAS*, 438, 3465
- Tempel, E., Tago, E., Liivamägi, L. J., 2012, *A&A*, 540, A106
- Tempel, E., Tamm, A. 2015, *A&A*, 576, L5
- Tojeiro, R., Masters, K. L., Richards, J. 2013, *MNRAS*, 432, 359
- Tovmassian, H. M. & Plionis, M. 2009, *ApJ*, 696, 1441
- Troxel M. A., Ishak M., 2014, preprint *arXiv*:1047.6990
- van den Bosch, F. C., 1998, *ApJ*, 507, 601
- Wang, Y., Yang, X., Mo, H. J., Li, C., van den Bosch, F. C., Fan, Z., Chen, X. 2008, *MNRAS*, 385, 1511
- Kang X., Wang P., 2015, *ApJ*, 813, 6
- Wang P., Kang X., 2017, *MNRAS*, 468, L123
- Wang P., Kang X., 2018, *MNRAS*, 473, 1562
- Wang P., Libeskind N. I., Tempel E., Kang X., Guo Q., 2021, *Nature Astronomy*, 5, 839
- Wang P., Guo Q., Libeskind N. I., Tempel E., Wei C., Kang X., 2019, *MNRAS*, 484, 4325
- Wang P., Kang X., Libeskind N. I., Guo Q., Gottlöber S., Wang W., 2020, *NewA*, 80, 101405
- Wang, P., Libeskind, N. I., Tempel, E., Pawłowski, M. S., Kang, X., Guo, Q. 2020, *ApJ*, 900, 129
- Wang P., Libeskind N. I., Pawłowski M. S., Kang X., Wang W., Guo Q., Tempel E., 2021, *ApJ*, 914, 78
- Wang, W., Wang, P., Guo, H., et al. 2024, *MNRAS*, 532, 4604
- Wang K., Avestruz C., Guo H., Wang W., Wang P., 2024, *MNRAS*, 532, 4616
- Wesson P. S., 1984, *A&A*, 138, 253
- West M. J., 1994, *MNRAS*, 268, 79
- Xu Y., Luo Y., Kang X., Li Z., Li Z., Wang P., Libeskind N., 2022, *ApJ*, 928, 100
- Zhang, Y., Yang, X., Wang, H., Wang, L., Mo, H. J., van den Bosch, F. C. 2013, *ApJ*, 779, 160
- Zhang, Y., Yang, X., Wang, H., et al. 2015, *ApJ*, 798, 17
- Zheng Y., Cai Y.-C., Zhu W., Neyrinck M., Wang P., Li S., 2023, *MNRAS*, 519, 1171